

# Extreme Suppression of Antiferromagnetic Order and Critical Scaling in a Two-Dimensional Random Quantum Magnet

Wenshan Hong,<sup>1,2</sup> Lu Liu,<sup>1</sup> Chang Liu,<sup>1,2</sup> Xiaoyan Ma,<sup>1,2</sup> Akihiro Koda,<sup>3,4</sup> Xin Li,<sup>5</sup> Jianming Song,<sup>5</sup> Wenyun Yang,<sup>6</sup> Jinbo Yang,<sup>6</sup> Peng Cheng,<sup>7</sup> Hongxia Zhang,<sup>7</sup> Wei Bao,<sup>7,8</sup> Xiaobai Ma,<sup>9</sup> Dongfeng Chen,<sup>9</sup> Kai Sun,<sup>9</sup> Wenan Guo,<sup>10,11</sup> Huiqian Luo,<sup>1,12</sup> Anders W. Sandvik,<sup>13,1,\*</sup> and Shiliang Li<sup>1,2,12,†</sup>

<sup>1</sup>Beijing National Laboratory for Condensed Matter Physics,

Institute of Physics, Chinese Academy of Sciences, Beijing 100190, China

<sup>2</sup>School of Physical Sciences, University of Chinese Academy of Sciences, Beijing 100190, China

<sup>3</sup>Institute of Materials Structure Science, High Energy Accelerator Research Organization (KEK-IMSS), 1-1 Oho, Tsukuba 305-0801, Japan

<sup>4</sup>Department of Materials Structure Science, Sokendai (The Graduate University for Advanced Studies), Tsukuba, Ibaraki, 305-0801, Japan

<sup>5</sup>Key Laboratory of Neutron Physics and Institute of Nuclear Physics and Chemistry,

China Academy of Engineering Physics, Mianyang 621999, China

<sup>6</sup>State Key Laboratory for Mesoscopic Physics, School of Physics, Peking University, Beijing, 100871, China

<sup>7</sup>Department of Physics and Beijing Key Laboratory of Opto-electronic Functional Materials & Micro-nano Devices, Renmin University of China, Beijing 100872, China

<sup>8</sup>Department of Physics, City University of Hong Kong, Kowloon, Hong Kong

<sup>9</sup>Department of Nuclear Physics, China Institute of Atomic Energy, Beijing, 102413, China

<sup>10</sup>Department of Physics, Beijing Normal University, Beijing 100875, China

<sup>11</sup>Beijing Computational Science Research Center, Beijing 100193, China

<sup>12</sup>Songshan Lake Materials Laboratory, Dongguan, Guangdong 523808, China

<sup>13</sup>Department of Physics, Boston University, 590 Commonwealth Avenue, Boston, Massachusetts 02215, USA

(Dated: July 24, 2020)

$\text{Sr}_2\text{CuTeO}_6$  is a square-lattice Néel antiferromagnet with superexchange between first-neighbor  $S = 1/2$  Cu spins mediated by plaquette centered Te ions. Substituting Te by W, the affected impurity plaquettes have predominantly second-neighbor interactions, thus causing local magnetic frustration. Here we report a study of  $\text{Sr}_2\text{CuTe}_{1-x}\text{W}_x\text{O}_6$  using neutron diffraction and  $\mu\text{SR}$  techniques, showing that the Néel order vanishes already at  $x = 0.025 \pm 0.005$ . We explain this extreme order suppression using a two-dimensional Heisenberg spin model, demonstrating that a W-type impurity induces a deformation of the order parameter that decays with distance as  $1/r^2$  at temperature  $T = 0$ . The associated logarithmic singularity leads to loss of order for any  $x > 0$ . Order for small  $x > 0$  and  $T > 0$  is induced by weak interplane couplings. In the nonmagnetic phase of  $\text{Sr}_2\text{CuTe}_{1-x}\text{W}_x\text{O}_6$ , the  $\mu\text{SR}$  relaxation rate exhibits quantum critical scaling with a large dynamic exponent,  $z \approx 3$ , consistent with a random-singlet state.

A central theme in modern condensed matter physics is the evolution of two-dimensional (2D) quantum antiferromagnets upon doping, as epitomized by the high- $T_c$  cuprates with charge carriers introduced into the  $\text{CuO}_2$  layers through off-layer doping [1, 2]. In-plane static impurities have also been studied, e.g., non-magnetic Zn substituting the spin  $S = 1/2$  carrying Cu ions [3–5]. In general, impurities and random frustrated couplings in a quantum magnet will eventually destroy any order and may induce not yet fully understood disordered states, e.g., quantum spin glasses [6–8], spin fluids [9], valence-bond glasses [10, 11], and random-singlet (RS) states [12–24].

We here report  $\mu\text{SR}$  and neutron diffraction experiments on  $\text{Sr}_2\text{CuTe}_{1-x}\text{W}_x\text{O}_6$ , which at  $x = 0$  realizes the 2D  $S = 1/2$  antiferromagnetic (AFM) Heisenberg model with predominantly first-neighbor interactions  $J_1$  generated through superexchange via Te ions at the centers of the plaquettes of  $2 \times 2$  Cu ions [25, 26]; see Fig. 1(a). At  $x = 1$ , the W ions instead mediate second-neighbor superexchange in the affected plaquettes, Fig. 1(b), with  $J_2 \approx J_1$  [27–29]. An intriguing magnetically disordered state exists within a window  $[x_{c1}, x_{c2}]$ ,

with  $x_{c1} \approx 0.1$  and  $x_{c2} \approx 0.6$  estimated [30–32]. The ability to tune the disorder and frustration by  $x$  offers unique opportunities to systematically study frustrated plaquette impurities of the  $J_2$  type illustrated in Fig. 1(c) for small  $x$  and the subsequent randomness-induced non-magnetic state for larger  $x$ .

We here demonstrate destruction of the Néel order in  $\text{Sr}_2\text{CuTe}_{1-x}\text{W}_x\text{O}_6$  at  $x_{c1} = 0.025 \pm 0.005$ , far below the previous estimate. We explain this dramatic order suppression using a classical Heisenberg model with random W and Te

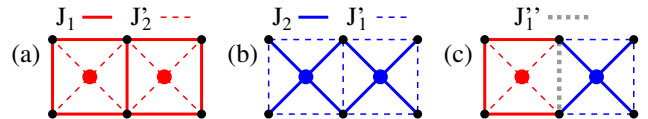


Figure 1. 2D Heisenberg couplings  $J_{ij}\mathbf{S}_i \cdot \mathbf{S}_j$  in  $\text{Sr}_2\text{CuTe}_{1-x}\text{W}_x\text{O}_6$ . The small black circles represent the  $S = 1/2$  carrying Cu ions, while red and blue circles correspond to Te and W ions, respectively. The dominant couplings mediated by Te in (a) and W in (b) are first-neighbor  $J_1$  (solid red lines) and second-neighbor  $J_2$  (solid blue lines), with  $J_1 \approx J_2 \approx 8$  meV [30, 33]. The couplings  $J'_1$  and  $J'_2$  indicated by the thin dashed lines are roughly 10% of the dominant couplings. The first-neighbor coupling  $J'_1$  on links between Te and W ions, the gray dashed line in (c), is about 4% of  $J_1$  [33].

\* sandvik@bu.edu

† slli@iphy.ac.cn

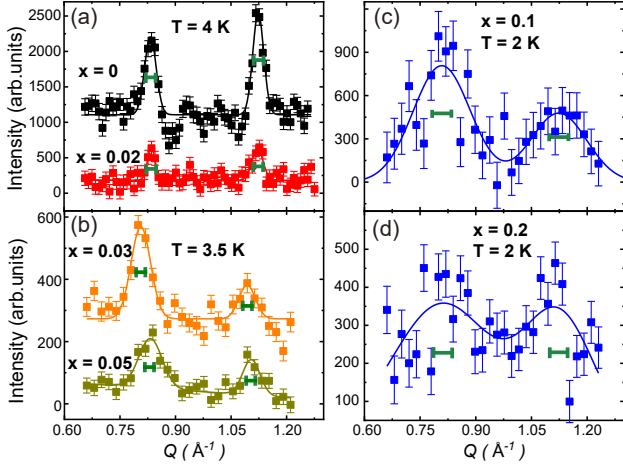


Figure 2. Neutron diffraction results for (a)  $x = 0$  and 0.02, (b) 0.03 and 0.05 (c) 0.1, and (d) 0.2. The peaks correspond to wave-vectors  $q = (1/2, 1/2, 0)$  and  $(1/2, 1/2, 1)$  in the tetragonal magnetic Brillouin zone, indicating dominant Néel AFM order ( $x = 0$  and 0.02) and short-range correlations ( $x \geq 0.03$ ). Data at  $T = 40$  K have been subtracted as background. The  $x = 0$  and 0.03 values have been shifted vertically for clarity. The curves are Gaussian fits and the green bars indicate the instrumental resolutions.

ions. Here 2D Néel order at temperature  $T = 0$  is destroyed even at infinitesimal  $x$ , due to a logarithmic singularity caused by the single-impurity deformation of the spin texture. Order at  $x > 0$  and  $T > 0$  is stabilized by weak inter-layer couplings. The columnar AFM state extending from  $x = 1$  is much more robust, which also can be explained by the classical model. In the non-magnetic phase, the neutron diffraction measurements reveal short-range Néel correlations and the  $\mu$ SR relaxation rate exhibits quantum-critical scaling with dynamic exponent  $z > 2$ , both consistent with recent predictions for the 2D RS state [22, 23].

**Experiments.**—Polycrystalline  $\text{Sr}_2\text{CuTe}_{1-x}\text{W}_x\text{O}_6$  samples were synthesized as described previously [25–27, 29]. The experiments were carried out at J-PARC ( $\mu$ SR) and China Advanced Research Reactor and Key Laboratory of Neutron Physics and Institute of Nuclear Physics and Chemistry, China (neutron diffraction); see also Supplemental Material [34].

Figure 2 shows our neutron diffraction results. Resolution limited magnetic peaks are observed at  $x = 0$  in Fig. 2(a), consistent with Néel AFM order [25, 30]. We have also confirmed (Supplemental Material [34]) columnar AFM order [31, 32] for  $x \in [0.7, 1]$ . The W doped sample with  $x = 0.02$ , Fig. 2(a), is still ordered, with resolution limited peaks (corresponding to a correlation length  $> 180 \text{ \AA} \approx 35$  lattice spacings). The broader peaks for  $x \geq 0.03$  in Figs. 2(b)–2(d) indicate the loss of long-range order between  $x = 0.02$  and 0.03. At  $x = 0.1$  the correlation length is still about  $40 \text{ \AA}$ .

The  $\mu$ SR asymmetry  $A(t)$  was fitted to

$$A(t) = A_0 \exp(-\lambda t) G_z(t) + A_{\text{BG}}, \quad (1)$$

where  $A_0$  is the initial asymmetry,  $\lambda$  the relaxation rate of the muon spins,  $A_{\text{BG}}$  the constant background, and  $G_z(t)$  the

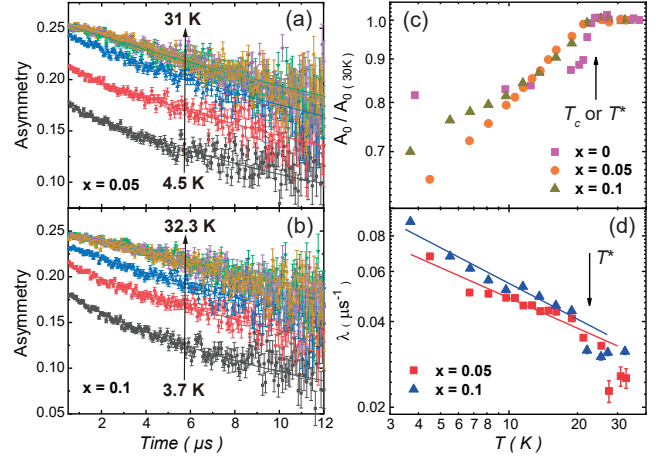


Figure 3. Time-dependent zero-field  $\mu$ SR spectra for (a)  $x = 0.05$  and (b)  $x = 0.1$  samples at different temperatures (the highest and lowest indicated) along with fits to Eq. (1). (c) Temperature dependent  $\mu$ SR asymmetry for  $x = 0, 0.05$ , and  $0.1$ , normalized by the values at  $T = 30$  K. (d) Temperature dependent relaxation rate  $\lambda$  for  $x = 0.05$  and  $0.1$ . The fitted lines correspond to critical scaling,  $\lambda \approx T^{-\gamma}$ , with  $\gamma = 0.35 \pm 0.03$  ( $x = 0.05$ ) and  $0.42 \pm 0.03$  ( $x = 0.1$ ).

Kubo-Toyabe function [35]. The function  $A(t)$  cannot actually describe the complete muon spectra of the magnetically ordered samples. It has already been shown that, for columnar AFM ordered systems at  $x = 1, 0.9$ , and  $0.8$ , the asymmetry initially drops very rapidly and oscillates [28, 32]. These features take place within  $1 \mu\text{s}$ , beyond the resolution of our measurements. Instead, Eq. (1) describes the relaxation at longer times and  $A_0$  is close to the asymmetry after the rapid initial drop. While the fits of Eq. (1) are not perfect for the long-range ordered samples (Supplemental Material [34]), the form describes the data for  $x = 0.05$  and  $0.1$  very well, as shown in Figs. 3(a) and 3(b).

The temperature dependent  $A_0$  is graphed in Fig. 3(c) for  $x = 0, 0.05$  and  $0.1$ . A sharp change is observed at the previously known ordering temperature  $T_c$  at  $x = 0$  [25, 26]. In contrast, in the  $x = 0.05$  and  $0.1$  samples  $A_0$  only decreases slowly below a characteristic temperature  $T^*$ . This behavior reflects gradual changes of the local fields as a result of the onset of short-range magnetic correlations but no ordering, which is consistent with the neutron results in Figs. 2(b) and 2(c). It should be noted that the value of  $A_0$  for  $x = 0$  at low temperatures is about  $4/5$  of that above  $T_c$ , while in the case of  $x = 1$  it is only  $1/3$  [27, 34]. It is beyond the scope of this work to explain the detailed form of  $A_0$ ; some additional analysis is provided in Supplementary Material [34].

Fig. 3(d) shows the temperature dependence of the relaxation rate  $\lambda$  for  $x = 0.05$  and  $0.1$ . Power-law behaviors reflect quantum-critical scaling in what is likely the RS phase. As explained in Supplemental Material, standard scaling arguments [36, 37] in combination with a constraint imposed by the recently discovered  $1/r^2$  form of the spin correlations in the 2D RS phase [22–24] can be used to derive the form  $\lambda \propto T^{-\gamma}$  with  $\gamma = 1 - 2/z$ , where  $z$  is the dynamic exponent. The values of  $\gamma$  extracted from the fits in Fig. 3(d) correspond to

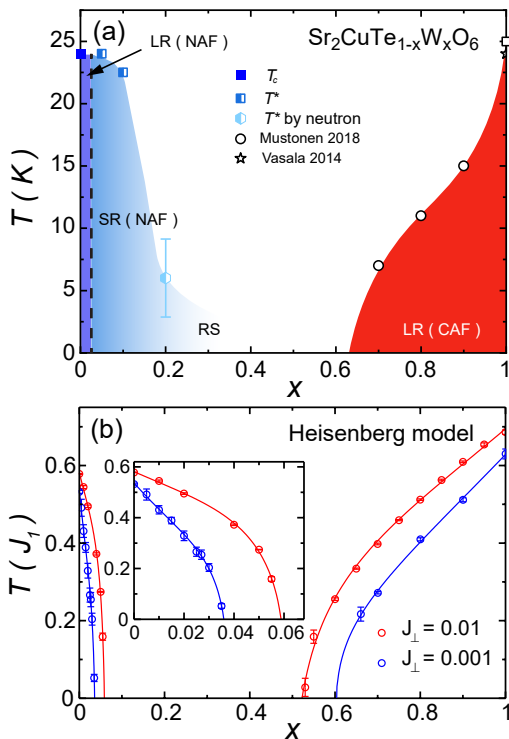


Figure 4. (a) Magnetic phase diagram of  $\text{Sr}_2\text{CuTe}_{1-x}\text{W}_x\text{O}_6$ . NAF and CAF denote Néel and columnar AFM correlations, respectively, either short-range (SR) or long-range (LR). The ordering temperature  $T_c$  and characteristic short-range correlation temperature  $T^*$  were determined by  $\mu\text{SR}$  measurements, except for  $T^*$  of the  $x = 0.2$  sample, which was obtained (Supplemental Material [34]) by neutron diffraction (b) Transition temperatures of the classical Heisenberg model of coupled layers, determined using Monte Carlo simulations. In the notation of Fig. 1 the 2D couplings are  $J_1 = J_2 = 1$ ,  $J'_1 = J'_2 = 0.1$ , and  $J''_1 = 0$ . Two different interlayer couplings are used;  $J_\perp = 10^{-2}$  and  $10^{-3}$ . Curves are drawn through the data points as guides to the eye.

$z = 3.0 \pm 0.2$  for  $x = 0.05$  and  $z = 3.5 \pm 0.3$  for  $x = 0.1$ . These values conform with the expectations in the RS phase, where  $z$  equals 2 at the Néel–RS transition and grows upon moving into the RS phase [22]. It should be noted that the value of  $A_{\text{BG}}$  in Eq. (1) somewhat affects the determination of  $\gamma$  but we consistently find power law behavior of  $\lambda$  and  $z(x = 0.1) > z(x = 0.05)$  (further discussed in Supplemental Material [34]). We note that the low-temperature  $\mu\text{SR}$  relaxation in quasi-2D spin glasses is very different [38].

Combining our  $\mu\text{SR}$  and neutron results with previous works, the magnetic phase diagram of  $\text{Sr}_2\text{CuTe}_{1-x}\text{W}_x\text{O}_6$  is shown in Fig. 4(a). The columnar order at  $x = 1$  is robust even for large Te substitution, which is indicative of only minor effects of magnetic frustration and remaining large connected ordered regions. The mean order parameter may then be gradually reduced in a way similar to diluted systems [39]. In contrast, introducing W in the  $x = 0$  sample rapidly destroys the Néel order at  $x_{c1} = 0.025 \pm 0.005$ . Short-range correlations with Néel structure still remain at low temperatures even

at  $x = 0.2$  based on our neutron-diffraction experiments and likely persist throughout what we argue is the 2D RS phase.

*Modeling.*—The width of the Néel phase in Fig. 4(a) is less than  $1/3$  of the previous estimates [30–32]. The Néel phase at finite W doping being narrower than the columnar phase at finite Te doping can be understood already at the classical level with the dominant Heisenberg coupling constants  $J_1$  and  $J_2$  in Fig. 1: Introducing a single Te impurity in the  $J_2$ -coupled columnar system, we simply lose the  $J_2$  couplings in the affected plaquette and there is only weak frustration from the much smaller  $J'_1$  and  $J''_1$  couplings. However, with a W impurity in the  $J_1$ -dominated Néel state the two new  $J_2$  bonds are completely frustrated. To quantitatively understand the extremely narrow Néel phase requires further insights.

Ideally, we would like to carry out calculations with the full quantum mechanical Heisenberg Hamiltonian. Even though progress has been made on some frustrated 2D quantum magnets with density-matrix renormalization group (DMRG) [40] and tensor-product [41] methods, including Heisenberg systems with random couplings [24], in practice calculations for frustrated systems are still challenging and it would be hard to extract a reliable phase diagram. However, we have found that already the classical Heisenberg model can explain the extreme fragility of the Néel state to W-plaquette impurities and also gives an overall reasonable phase diagram.

The long-range Néel order at  $T = 0$  in the 2D Heisenberg model with uniform exchange  $J_1 \mathbf{S}_i \cdot \mathbf{S}_j$  on all first neighbors  $(i, j)$  is destroyed by thermal fluctuations at  $T > 0$  [42, 43]. In weakly coupled planes of classical or quantum spins,  $T_c \propto J_1 \ln^{-1}(J_1/J_\perp)$ , where  $J_\perp$  is the coupling between spins in adjacent planes [44, 45]. Since a quantum magnet with AFM order or a long correlation length behaves in many respects as a “renormalized classical” system [43], the initial effects of doping the  $x = 0$  and  $x = 1$  system should be captured correctly by a classical model, up to  $O(1)$  factors.

In the notation of Fig. 1, we set the 2D couplings to  $J_1 = J_2 = 1$ ,  $J'_1 = J'_2 = 0.1$ , and  $J''_1 = 0$ , with  $|\mathbf{S}_i| = 1$ . For coupled planes we consider  $J_\perp = 10^{-2}$  and  $10^{-3}$ . We used standard Monte Carlo methods for frustrated Heisenberg models [46, 47], with Binder cumulant techniques [48] for extracting  $T_c$  at fixed  $x$ , based on averages over several hundred realizations of the random W and Te plaquettes on systems with up to  $72 \times 72 \times 18$  spins. The resulting infinite-size extrapolated phase boundaries are shown in Fig. 4(b). When comparing with the experiments, it should be noted that  $T = 25$  K corresponds roughly to 0.3 in units of  $J_1$  and that  $T_c$  in uniform coupled  $S = 1/2$  planes with  $J_\perp$  of order  $10^{-2}$  is lower by about 50% than our classical result at  $x = 0$  [45]. We expect quantum fluctuations to shrink the ordered phases also in the  $x$  direction, and the differences between the numerical and experimental results for the columnar phase boundary should also be due to quantum effects (and possibly weak interactions beyond those included here).

As seen in Fig. 4(b), upon changing  $J_\perp$  from  $10^{-2}$  to  $10^{-3}$ ,  $T_c$  at  $x = 0$  is only slightly reduced, as expected on account of the logarithmic form discussed above. For  $x > 0$  the phase boundary drops more rapidly to zero for the smaller  $J_\perp$ , and the size of the Néel phase is substantially smaller. A very

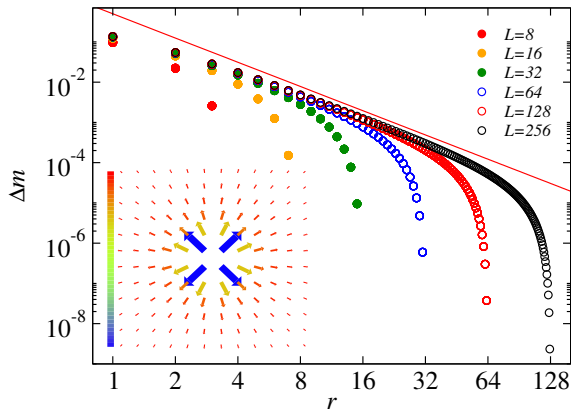


Figure 5. Deformation of the order parameter of the classical Heisenberg model with a W-type plaquette impurity as defined in Fig. 1, with the same couplings as in Fig. 4. The deviation  $\Delta m = 1 - |S_z^i|$ , where the  $z$  direction is that of the bulk Néel order, is shown vs the distance  $r$  from the impurity along the  $(1, 0)$  lattice direction for several system sizes. The line shows the form  $1/r^2$ . The inset shows the projection of the spins to the  $xy$  spin plane, with the color coding corresponding to  $m \in [0.49, 1]$ . The magnitude of the  $xy$  component decays as  $1/r$  from its maximal value  $\approx 0.87$  closest to the impurity. The behaviors correspond to an angular distortion  $\propto 1/r$ .

narrow Néel phase with high sensitivity of the  $T = 0$  transition point to  $J_\perp$  is not expected within a simple picture of conventional local impurity suppression of the order [39]. We therefore investigate the deformation of the Néel order around a single impurity plaquette at  $T = 0$ , which we have done by minimizing the energy with a combination of simulated annealing and energy conserving spin moves.

The deviation  $\Delta m$  of the local ordered moment from the bulk value is graphed in Fig. 5 versus the distance  $r$  from the impurity. The form  $\Delta m \propto 1/r^2$  causes a logarithmic divergence when integrated over  $r$  (but the total energy cost of the deformation stays constant, with the energy density decaying as  $1/r^4$ ). This single-impurity response suggests that any impurity fraction  $x > 0$  destroys the long-range order, and this is demonstrated explicitly in the Supplemental Material [34]. A similar fragility of non-collinear bulk order in the presence of certain impurities was previously pointed out [8], but the profound impact of the plaquette impurity (which can be understood as a composite of two dipoles; see Supplemental Material [34]) on the collinear Néel state had not been anticipated.

For the weakly coupled planes in Fig. 4(b), the Néel order is stabilized for a range of  $x > 0$  depending on  $J_\perp/J_1$ , but we have not studied the functional form of  $x_{c1}$  versus  $J_\perp$ . The disorder should be irrelevant at the  $T > 0$  phase transitions according to the Harris criterion [49, 50], and we expect standard three-dimensional O(3) universality. We do not have sufficient data for large systems to test the critical exponents. In an  $S = 1/2$  system such as  $\text{Sr}_2\text{CuTe}_{1-x}\text{W}_x\text{O}_6$ , quantum fluctuations should further suppress the order and reduce  $x_{c1}$ , and we expect the same type of logarithmic singularity as in the classical case when  $J_\perp/J_1 \rightarrow 0$ , on account of the renormalized classical picture of the quantum Néel state [43].

*Discussion.*—The extreme effect of the W impurities in the

Néel state was not captured by the density functional calculations in Ref. [32], which suggested destabilization of the Néel order for  $x \approx 0.1-0.2$  in  $\text{Sr}_2\text{CuTe}_{1-x}\text{W}_x\text{O}_6$ , significantly above  $x_{c1} \approx 0.025$  found in our experiments. The mechanism we have uncovered here relies on a singular effect of frustrated plaquette impurities in 2D, with weak 3D couplings pushing the transition from  $x = 0$  to to small  $x > 0$ .

Once the Néel order vanishes, from the classical perspective a spin glass phase is expected [8, 51]. In the presence of strong quantum fluctuations in  $S = 1/2$  systems, there is mounting evidence from model studies that the spin glass can be supplanted by an RS state [8, 19, 22–24]. A particular realization of the RS state amenable to large-scale quantum Monte Carlo calculations exhibits criticality with a dynamic exponent  $z \geq 2$  and dominant Néel-type spin correlations decaying with distance as  $1/r^2$  at  $T = 0$  [22, 23]. This form of the correlations was recently confirmed in a frustrated random-bond system with DMRG calculations [24], thus further supporting universal RS behavior. The significant staggered correlations well past the Néel phase in  $\text{Sr}_2\text{CuTe}_{1-x}\text{W}_x\text{O}_6$ , as revealed by our neutron diffraction experiments at  $x = 0.1$  and  $0.2$ , are thus expected within the RS scenario. Previous results at  $x = 0.5$  also showed remnants of Néel correlations [33]. We here further demonstrated quantum-critical scaling of the  $\mu\text{SR}$  relaxation rate with varying  $z > 2$ , as recently predicted in the 2D RS state [22, 23].

It would be interesting to further test the proposed RS scaling forms experimentally in  $\text{Sr}_2\text{CuTe}_{1-x}\text{W}_x\text{O}_6$ . A re-analysis [22] of susceptibility data for  $x \geq 0.2$  [31] supported the predicted form  $\chi \propto T^{-\gamma}$  with  $\gamma < 1$ . Detailed inelastic neutron scattering studies would be very useful, but our attempts to grow large single-crystals have so far not been successful. With polycrystalline samples, NMR experiments may be able to further elucidate the nature of the RS state and the Néel–RS transition. RS signatures were previously reported in  $\text{YbMgGaO}_4$  [20] and  $\alpha\text{-Ru}_{1-x}\text{Ir}_x\text{Cl}_3$  [52], but in addition to random frustration these materials have Dzyaloshinskii-Moriya interactions and spin vacancies, respectively. Beyond its intrinsic importance, the 2D RS state should also be a useful benchmark for experiments on potential uniform spin liquids [53, 54], where it is often difficult [11, 20, 55, 56] to distinguish between impurity physics and theoretically predicted properties of clean systems.

## ACKNOWLEDGMENTS

*Acknowledgments.*—W.H. and L.L. contributed equally to this work. We would like to thank Oleg Sushkov for valuable comments. The research at Chinese institutions is supported by the National Key R&D Program of China (Grants No. 2017YFA0302900, No. 2016YFA0300502, No. 2018YFA0704201, No. 2016YFA0300604, No. 2017YFA0303100), the National Natural Science Foundation of China (Grants No. 11734002, No. 11775021, No. 11874401, No. 11874401, No. 11674406, No. 11822411, No. 12061130200, No. 11227906), and by the Strategic Priority Research Program (B) of the Chinese Academy of

Sciences (Grants No. XDB25000000, No. XDB07020000, No. XDB28000000, No. XDB33010100). H.L. is grateful for support from the Youth Innovation Promotion Association of CAS (Grant No. 2016004) and Beijing Natural Science Foundation (Grant No. JQ19002). The work in Boston was supported by the NSF under Grant No. DMR-1710170 and

by the Simons Foundation under Simons Investigator Award No. 511064. L.L. would like to thank Boston University's Condensed Matter Theory Visitors Program for support. We also acknowledge the Super Computing Center of Beijing Normal University and Boston University's Research Computing Services for their support.

- 
- [1] P. A. Lee, N. Nagaosa, and X.-G. Wen, Doping a Mott insulator: Physics of high-temperature superconductivity, *Rev. Mod. Phys.* **78**, 17 (2006).
- [2] S. Chatterjee, S. Sachdev, and M. S. Scheurer, Intertwining Topological Order and Broken Symmetry in a Theory of Fluctuating Spin-Density Waves, *Phys. Rev. Lett.* **119**, 227002 (2017).
- [3] O. P. Vajk, P. K. Mang, M. Greven, P. M. Gehring, and J. W. Lynn, Quantum impurities in the two-dimensional spin one-half Heisenberg antiferromagnet, *Science* **295**, 1691 (2002).
- [4] A. W. Sandvik, Classical percolation transition in the diluted two-dimensional  $S=1/2$  Heisenberg antiferromagnet, *Phys. Rev. B* **66**, 024418 (2002).
- [5] C.-W. Liu, S. Liu, Y.-J. Kao, A. L. Chernyshev, and A. W. Sandvik, Impurity-Induced Frustration in Correlated Oxides, *Phys. Rev. Lett.* **102**, 167201 (2009).
- [6] J. Ye, S. Sachdev, and N. Read, Solvable spin glass of quantum rotors, *Phys. Rev. Lett.* **70**, 4011 (1993).
- [7] J. Oitmaa and O.P. Sushkov, Two-Dimensional Randomly Frustrated Spin-1/2 Heisenberg Model, *Phys. Rev. Lett.* **87**, 167206 (2001).
- [8] S. Dey, E. C. Andrade, and M. Vojta, Destruction of long-range order in noncollinear two-dimensional antiferromagnets by random-bond disorder, *Phys. Rev. B* **101**, 020411(R) (2020).
- [9] S. Sachdev and J. Ye, Gapless spin-fluid ground state in a random quantum Heisenberg magnet, *Phys. Rev. Lett.* **70**, 3339 (1993).
- [10] M. Tarzia, G. Biroli, The Valence Bond Glass phase, *Europhys. Lett.* **82**, 67008 (2008).
- [11] R. R. P. Singh, Valence Bond Glass Phase in Dilute Kagome Antiferromagnets, *Phys. Rev. Lett.* **104**, 177203 (2010).
- [12] R. N. Bhatt and P. A. Lee, Scaling Studies of Highly Disordered Spin-1/2 Antiferromagnetic Systems, *Phys. Rev. Lett.* **48**, 344 (1982).
- [13] D. S. Fisher, Random antiferromagnetic quantum spin chains, *Phys. Rev. B* **50**, 3799 (1994).
- [14] O. Motrunich, S.-C. Mau, D. A. Huse, and D. S. Fisher, Infinite-Randomness Quantum Ising Critical Fixed Points, *Phys. Rev. B* **61**, 1160 (2000).
- [15] Y.-C. Lin, R. Mélin, H. Rieger, and F. Iglói, Low-Energy Fixed Points of Random Heisenberg Models, *Phys. Rev. B* **68**, 024424 (2003).
- [16] C. R. Laumann, D. A. Huse, A. W. W. Ludwig, G. Refael, S. Trebst, and M. Troyer, Strong-disorder renormalization for interacting non-Abelian anyon systems in two dimensions, *Phys. Rev. B* **85**, 224201 (2012).
- [17] K. Watanabe, H. Kawamura, H. Nakano, and T. Sakai, Quantum Spin-Liquid Behavior in the Spin-1/2 Random Heisenberg Antiferromagnet on the Triangular Lattice, *J. Phys. Soc. Jpn.* **83** 034714 (2014).
- [18] K. Uematsu, H. Kawamura, Randomness-induced quantum spin liquid behavior in the  $s = \frac{1}{2}$  random  $J_1$ - $J_2$  Heisenberg antiferromagnet on the square lattice, *Phys. Rev. B*, **98**, 134427 (2018).
- [19] I. Kimchi, A. Nahum, and T. Senthil, Valence Bonds in Random Quantum Magnets: Theory and Application to  $\text{YbMgGaO}_4$ , *Phys. Rev. X* **8**, 031028 (2018).
- [20] I. Kimchi, J. P. Sheckelton, T. M. McQueen, and P. A. Lee, Scaling and data collapse from local moments in frustrated disordered quantum spin systems, *Nat. Comm.* **9**, 4367 (2018).
- [21] H. Kawamura and K. Uematsu, Nature of the randomness-induced quantum spin liquids in two dimensions, *J. Phys. Condens. Matter* **31**, 504003 (2019).
- [22] L. Liu, H. Shao, Y.-C. Lin, W. Guo, and A. W. Sandvik, Random-Singlet Phase in Disordered Two-Dimensional Quantum Magnets, *Phys. Rev. X* **8**, 041040 (2018).
- [23] L. Liu, W. Guo, and A. W. Sandvik, Quantum-critical scaling properties of the two-dimensional random-singlet state, *Phys. Rev. B* **102**, 054443 (2020).
- [24] H.-D. Ren, T.-Y. Xiong, H.-Q. Wu, D. N. Sheng, and S.-S. Gong, Characterizing random-singlet state in two-dimensional frustrated quantum magnets and implications for the double perovskite  $\text{Sr}_2\text{CuTe}_{1-x}\text{W}_x\text{O}_6$ , arXiv:2004.02128.
- [25] T. Koga, N. Kurita, M. Avdeev, S. Danilkin, T. J. Sato, and H. Tanaka, Magnetic structure of the  $S = \frac{1}{2}$  quasi-two-dimensional square-lattice Heisenberg antiferromagnet  $\text{Sr}_2\text{CuTeO}_6$ , *Phys. Rev. B* **93**, 054426 (2016).
- [26] P. Babkevich, V. M. Katukuri, B. Fåk, S. Rols, T. Fennell, D. Pajić, H. Tanaka, T. Pardini, R. R. P. Singh, A. Mitrushchenkov, O. V. Yazyev, and H. M. Rønnow, Magnetic Excitations and Electronic Interactions in  $\text{Sr}_2\text{CuTeO}_6$ : A Spin-1/2 Square Lattice Heisenberg Antiferromagnet, *Phys. Rev. Lett.* **117**, 237203 (2016).
- [27] S. Vasala, M. Avdeev, S. Danilkin, O. Chmaissem, and M. Karppinen, Magnetic structure of  $\text{Sr}_2\text{CuWO}_6$ , *J. Phys.: Condens. Matter* **26**, 496001 (2014).
- [28] S. Vasala, H. Saadaoui, E. Morenzoni, O. Chmaissem, T.S. Chan, J.-M. Chen, Y.-Y. Hsu, H. Yamauchi, and M. Karppinen, Characterization of magnetic properties of  $\text{Sr}_2\text{CuWO}_6$  and  $\text{Sr}_2\text{CuMoO}_6$ , *Phys. Rev. B*, **89**, 134419 (2014).
- [29] H. C. Walker, O. Mustonen, S. Vasala, D. J. Voneshen, M. D. Le, D. T. Adroja, and M. Karppinen, Spin wave excitations in the tetragonal double perovskite  $\text{Sr}_2\text{CuWO}_6$ , *Phys. Rev. B* **94**, 064411 (2016).
- [30] O. Mustonen, S. Vasala, E. Sadrollahi, K. P. Schmidt, C. Baines, H. C. Walker, I. Terasaki, F. J. Litterst, E. Baggio-Saitovitch, and M. Karppinen, Spin-liquid-like state in a spin-1/2 square-lattice antiferromagnet perovskite induced by  $d^{10}$ - $d^0$  cation mixing, *Nat. Commun.* **9**, 1085 (2018).
- [31] M. Watanabe, N. Kurita, H. d Tanaka, W. Ueno, K. Matsui, and T. Goto, Valence-bond-glass state with a singlet gap in the spin- $\frac{1}{2}$  square-lattice random  $J_1$ - $J_2$  Heisenberg antiferromagnet  $\text{Sr}_2\text{CuTe}_{1-x}\text{W}_x\text{O}_6$ , *Phys. Rev. B* **98**, 054422 (2018).
- [32] O. Mustonen, S. Vasala, K. P. Schmidt, E. Sadrollahi, H. C. Walker, I. Terasaki, F. J. Litterst, E. Baggio-Saitovitch, M. and Karppinen, Tuning the  $S = 1/2$  square-lattice antiferromagnet  $\text{Sr}_2\text{Cu}(\text{Te}_{1-x}\text{W}_x)\text{O}_6$  from Néel order to quantum disorder to

- columnar order, Phys. Rev. B, **98**, 064411 (2018).
- [33] V. M. Katukuri, P. Babkevich, O. Mustonen, H. C. Walker, B. Fåk S. Vasala, M. Karppinen, H. M. Rønnow, and O. V. Yazyev, Exchange Interactions Mediated by Nonmagnetic Cations in Double Perovskites, Phys. Rev. Lett. **124**, 077202 (2020).
- [34] See Supplemental Material for experimental details, quantum-critical scaling forms, and additional Monte Carlo results, which includes references 57-62.
- [35] R. S. Hayano, Y. J. Uemura, J. Imazato, N. Nishida, T. Yamazaki, and R. Kubo, Zero-and low-field spin relaxation studied by positive muons, Phys. Rev. B **20**, 850 (1979).
- [36] M. P. A. Fisher, P. B. Weichman, G. Grinstein, and D. S. Fisher, Boson localization and the superfluid-insulator transition, Phys. Rev. B **40**, 546 (1989).
- [37] A. V. Chubukov and S. Sachdev, Universal Magnetic Properties of  $\text{La}_{2-\delta}\text{Sr}_\delta\text{CuO}_4$  at Intermediate Temperatures, Phys. Rev. Lett. **71**, 169 (1993).
- [38] P. Yadav, S. Sharma, P. J. Baker, P. K. Biswas, I. da Silva, R. Raghunathan, U. Deshpande, R. J. Choudhary, N. P. Lalla, and A. Banerjee,  $\mu\text{SR}$  and neutron diffraction studies on the tuning of spin-glass phases in the partially ordered double perovskites  $\text{SrMn}_{1-x}\text{W}_x\text{O}_3$ , Phys. Rev. B **99**, 214421 (2019).
- [39] M. F. Collins, *Magnetic Critical Scattering* (Oxford University Press, New York 1989).
- [40] R. Verresen, F. Pollmann, and R. Moessner, Quantum dynamics of the square-lattice Heisenberg model, Phys. Rev. B **98**, 155102 (2018).
- [41] L. Chen, D.-W. Qu, H. Li, B.-B. Chen, S.-S. Gong, J. von Delft, A. Weichselbaum, and W. Li, Two-temperature scales in the triangular-lattice Heisenberg antiferromagnet, Phys. Rev. B **99**, 140404(R) (2019).
- [42] N. D. Mermin and H. Wagner, Absence of Ferromagnetism or Antiferromagnetism in One- or Two-Dimensional Isotropic Heisenberg Models, Phys. Rev. Lett. **17**, 1133 (1966).
- [43] S. Chakravarty, B. I. Halperin, and D. R. Nelson, Two-dimensional quantum Heisenberg antiferromagnet at low temperatures, Phys. Rev. B **39**, 2344 (1989).
- [44] V. Y. Irkhin and A. A. Katanin, Thermodynamics of isotropic and anisotropic layered magnets: renormalization-group approach and  $1/N$  expansion. Phys. Rev. B **57**, 379 (1998).
- [45] P. Sengupta, A. W. Sandvik, and R. R. P. Singh, Specific heat of quasi-two-dimensional antiferromagnetic Heisenberg models with varying interplanar couplings, Phys. Rev. B **68**, 094423 (2003).
- [46] J. Alonso, A. A. tarancón, H. Ballestros, L. Fernández, V. Martín-Mayor, A. Muñoz Sudupe, Monte Carlo study of  $O(3)$  antiferromagnetic models in three dimensions, Phys. Rev. B **53**, 2537 (1996).
- [47] L. W. Lee and A. P. Young, Large-scale Monte Carlo simulations of the isotropic three-dimensional Heisenberg spin glass, Phys. Rev. B **76**, 024405 (2007).
- [48] A. W. Sandvik, Computational Studies of Quantum Spin Systems, AIP Conf. Proc. **1297**, 135 (2010).
- [49] A. B. Harris, Effect of random defects on the critical behaviour of Ising models, J. Phys. C **7**, 1671 (1974).
- [50] J. T. Chayes, L. Chayes, D. S. Fisher, and T. Spencer, Finite-size scaling and correlation lengths for disordered systems, Phys. Rev. Lett. **57**, 2999 (1986).
- [51] Y. Xu and D.-X. Yao, Spin glass in the bond-diluted  $J_1$ - $J_2$  Ising model on the square lattice, Phys. Rev. B **97**, 224419 (2018).
- [52] S.-H. Baek, H. W. Yeo, S.-H. Do, K.-Y. Choi, L. Janssen, M. Vojta and B. Büchner, Observation of a gapless spin liquid in a diluted Kitaev honeycomb material, Phys. Rev. B **102**, 094407 (2020).
- [53] L. Savary and L. Balents, Quantum spin liquids: a review, Rep. Prog. Phys. **80**, 016502 (2017).
- [54] Y. Zhou, K. Kanoda, and T.-K. Ng, Quantum spin liquid states, Rev. Mod. Phys. **89**, 025003 (2017).
- [55] Y. Li, G. Chen, W. Tong, L. Pi, J. Liu, Z. Yang, X. Wang, and Q. Zhang, Rare-Earth Triangular Lattice Spin Liquid: A Single-Crystal Study of  $\text{YbMgGaO}_4$ , Phys. Rev. Lett. **115**, 167203 (2015).
- [56] Z. Ma *et al.*, Spin-Glass Ground State in a Triangular-Lattice Compound  $\text{YbZnGaO}_4$ , Phys. Rev. Lett. **120**, 087201 (2018).
- [57] C. Slichter, *Principles of Magnetic Resonance*, 3rd ed. (Springer-Verlag, Berlin, Heidelberg, 1990).
- [58] Y.-R. Shu, M. Dupont, D.-X. Yao, S. Capponi, and A. W. Sandvik, Dynamical properties of the  $S = 1/2$  random Heisenberg chain, Phys. Rev. B **97**, 104424 (2018).
- [59] M. Randeria, N. Trivedi, A. Moreo, and R. T. Scalettar, Pairing and spin gap in the normal state of short coherence length superconductors, Phys. Rev. Lett. **69**, 2001 (1992).
- [60] O. P. Sushkov, Long-range dynamics related to magnetic impurities in the two-dimensional Heisenberg antiferromagnet, Phys. Rev. B **68**, 094426 (2003).
- [61] L. Lu, W. Guo, and A. W. Sandvik (in preparation).
- [62] J. Vannimenus, S. Kirkpatrick, F. D. M. Haldane, C. Jayaprakash, Ground-state morphology of random frustrated XY systems, Phys. Rev. B **39** 4634 (1989).

## Supplemental Material

## Extreme Suppression of Antiferromagnetic Order and Critical Scaling in a Two-Dimensional Quantum Magnet

Wenshan Hong,<sup>1,2</sup> Lu Liu,<sup>1</sup> Chang Liu,<sup>1,2</sup> Xiaoyan Ma,<sup>1,2</sup> Akihiro Koda,<sup>3,4</sup> Xin Li,<sup>5</sup> Jianming Song,<sup>5</sup> Wenyun Yang,<sup>6</sup> Peng Cheng,<sup>7</sup> Hongxia Zhang,<sup>7</sup> Wei Bao,<sup>7,8</sup> Xiaobai Ma,<sup>9</sup> Dongfeng Chen,<sup>9</sup> Kai Sun,<sup>9</sup> Wenan Guo,<sup>10,11</sup> Huiqian Luo,<sup>1,12</sup> Anders W. Sandvik,<sup>13,1,\*</sup> and Shiliang Li,<sup>1,2,12,†</sup>

<sup>1</sup> *Beijing National Laboratory for Condensed Matter Physics,*

*Institute of Physics, Chinese Academy of Sciences, Beijing 100190, China*

<sup>2</sup> *School of Physical Sciences, University of Chinese Academy of Sciences, Beijing 100190, China*

<sup>3</sup> *Institute of Materials Structure Science, High Energy Accelerator Research Organization (KEK-IMSS),  
1-1 Oho, Tsukuba 305-0801, Japan*

<sup>4</sup> *Department of Materials Structure Science, Sokendai (The Graduate University for Advanced Studies),  
Tsukuba, Ibaraki, 305-0801, Japan*

<sup>5</sup> *Key Laboratory of Neutron Physics and Institute of Nuclear Physics and Chemistry,  
China Academy of Engineering Physics, Mianyang 621999, China*

<sup>6</sup> *State Key Laboratory for Mesoscopic Physics, School of Physics, Peking University, Beijing, 100871, China*

<sup>7</sup> *Department of Physics and Beijing Key Laboratory of Opto-electronic Functional Materials & Micro-nano Devices,  
Renmin University of China, Beijing 100872, China*

<sup>8</sup> *Department of Physics, City University of Hong Kong, Kowloon, Hong Kong*

<sup>9</sup> *Department of Nuclear Physics, China Institute of Atomic Energy, Beijing, 102413, China*

<sup>10</sup> *Department of Physics, Beijing Normal University, Beijing 100875, China*

<sup>11</sup> *Beijing Computational Science Research Center, Beijing 100193, China*

<sup>12</sup> *Songshan Lake Materials Laboratory, Dongguan, Guangdong 523808, China*

<sup>13</sup> *Department of Physics, Boston University, 590 Commonwealth Avenue, Boston, Massachusetts 02215, USA*

\* e-mail: sandvik@bu.edu, † slli@iphy.ac.cn

We provide additional experimental (Sec. 1), theoretical (Sec. 2), and Monte Carlo simulation (Sec. 3) results supporting the conclusions of the main paper. Additional  $\mu$ SR  $A(t)$  data are presented in Sec. 1 A and the fitting procedures are explained. Neutron diffraction data in the columnar AFM state are presented in Sec. 1 B and in Sec. 1 C we explain how the cross-over temperature  $T^*$  was determined from the neutron data. In Sec. 2, we derive the scaling form of the  $\mu$ SR relaxation rate  $\lambda$ . In Sec. 3, we present additional Monte Carlo results for the classical 2D Heisenberg model with W-type impurities.

### 1. ADDITIONAL EXPERIMENTAL INFORMATION

Polycrystalline samples of  $\text{Sr}_2\text{CuTe}_{1-x}\text{W}_x\text{O}_6$  were synthesized from stoichiometric mixtures of SrO, CuO, TeO<sub>2</sub>, and WO<sub>3</sub> powders by the solid-state reaction method reported previously [25–27, 29]. The  $\mu$ SR experiments were performed at the S1 ARTEMIS spectrometer (Proposal No. 2018B0156), J-PARC, with the mini cryostat down to 4 K. The neutron-diffraction experiments were carried out at Bamboo ( $\lambda = 2.358 \text{ \AA}$ ) and Xingzhi ( $\lambda = 2.7302 \text{ \AA}$ ) triple-axis spectrometers, and at the PKU High-Intensity Powder Neutron Diffractometer ( $\lambda = 2.3 \text{ \AA}$ ) at China Advanced Research Reactor (CARR), and the Kumpeng triple-axis spectrometer ( $\lambda = 2.7302 \text{ \AA}$ ) at Key Laboratory of Neutron Physics and Institute of Nuclear Physics and Chemistry, China. Neutron speed velocity selectors were used before the monochromator with the Bamboo and Xingzhi spectrometers.

### A. Raw $\mu$ SR data

The time dependent asymmetry  $A(t)$  from our  $\mu$ SR experiments for  $x = 0$  and 1 are shown in Fig. S1. As discussed in the main text, the  $x = 0$  sample [Fig. S1(a)] has long-range Néel AFM order, while the  $x = 1$  sample [Fig. S1(b)] has long-range columnar order. It is clear that the fits by Eq. (1) are not good at low temperatures. This is in contrast with the good fits at  $x = 0.05$  and 0.1, as shown in Figs. 3(a) and 3(b).

The reason for the suboptimal fits at  $x = 0$  and 1 is that, in the ordered states, we need multiple relaxation rates to describe the data, as shown in Ref. [28]. Here we test the following simpler function:

$$A(t) = A_0[f + (1 - f)\exp(-\lambda t)]G_z(t) + A_{BG}. \quad (\text{S1})$$

Compared to the fitting function in the main text, the new function introduces a factor  $f$  to effectively account for a sec-

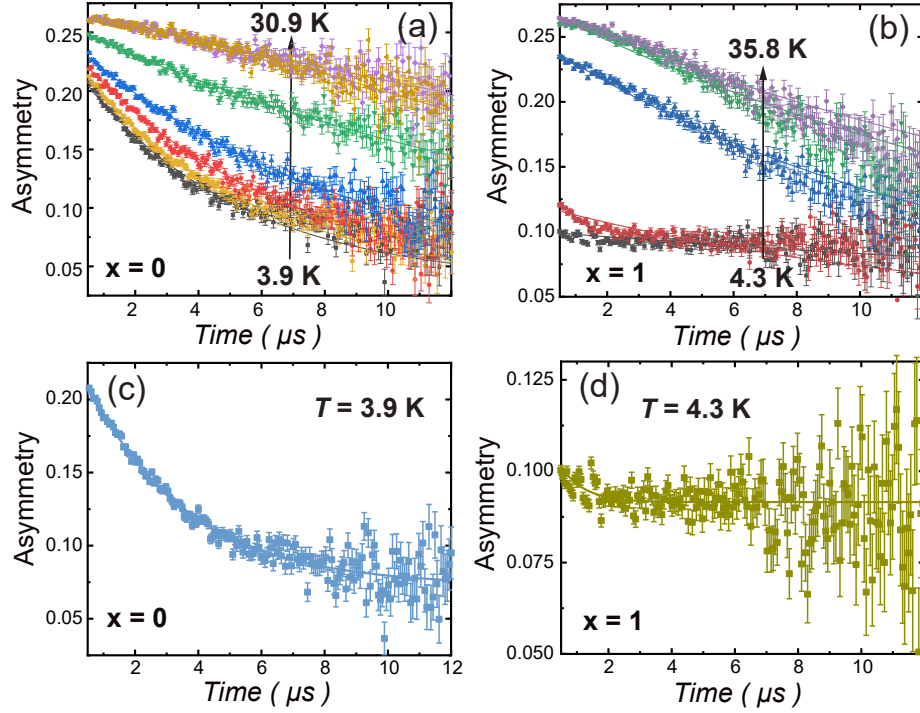


Figure S1. (a) and (b) show zero-field  $\mu$ SR spectra of  $\text{Sr}_2\text{CuTe}_{1-x}\text{W}_x\text{O}_6$  samples with  $x = 0$  and 1, respectively. Results for several temperatures are shown, with the highest and lowest indicated for both samples. The curves are fits to the form Eq. (1) with a single relaxation rate. (c) and (d) show the spectra for  $x = 0$  and 1, respectively, at the corresponding base temperatures. The curves are fits to the modified form Eq. (S1), which provides a better description of the data in the ordered state.

ond relaxation rate that is very small, so that its value is effectively zero on the time scale of the experiment. The very well fitted low-temperature results for  $x = 0$  and 1 are shown in Figs. S1(c) and S1(d). It is worth noting that  $f$  is close to  $1/3$  for  $x = 0$ , and  $1/2$  for  $x = 1$ . We stress that we need the modified fitting form only for analyzing the ordered samples. As noted in the main text and shown in Figs. 3(a) and 3(b), for the short-range correlated samples with  $x = 0.05$  and  $0.1$  the form Eq. (1) works essentially perfectly.

When fitting the  $\mu$ SR spectra, we have chosen a temperature-independent background  $A_{\text{BG}} = 0.035$  for all the samples. This value is derived from the fact that the value of  $A(t)$  at  $1 \mu\text{s}$  at base temperature is about  $1/3$  of that above  $T_c$ , as shown in Ref. [28]. The same instrument was used for all the  $\mu$ SR measurements and all the samples have similar mass and were mounted in similar holders. For all these reasons we expect that the background should be close to the same for all the samples. Reasonable fits can be obtained for  $A_{\text{BG}}$  ranging from 0 to 0.1, and using different values in this range does not affect the conclusion of low-temperature power-law scaling  $\lambda \sim T^{-\gamma}$  for  $x = 0.05$  and  $0.1$ ; the exponent changes only marginally and  $\gamma(0.1) > \gamma(0.05)$  always holds.

### B. Neutron diffraction results for the columnar AFM state

Neutron diffraction data for  $x$  from 0.7 to 1 are shown in Fig. S2. At these  $W$  fractions the system is expected from

previous studies [32] to have columnar AFM order at low temperature, which we confirm here with the resolution limited peaks at the corresponding wave-vectors.

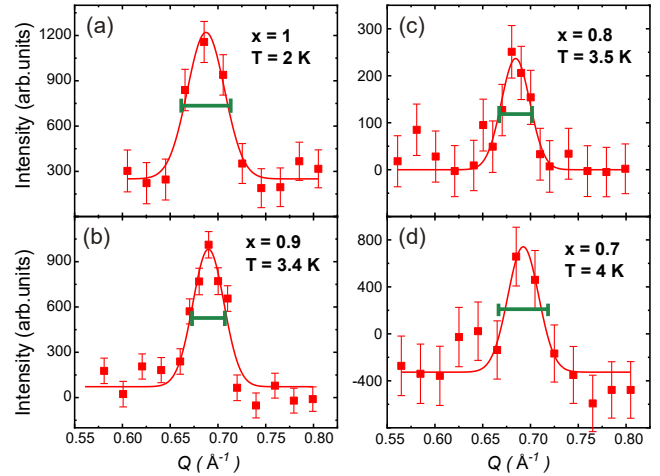


Figure S2. Neutron diffraction data along with Gaussian fits for  $x = 1$  (a) 0.9 (b), 0.8 (c), and 0.7 (d). The peak locations correspond to  $q = (0.5, 0, 0.5)$  and  $(0, 0.5, 0.5)$ , i.e., columnar AFM structure. The temperature is indicated in each panel and data taken at  $T = 40$  K have been subtracted as background contributions. The green bars indicate the instrumental resolution.



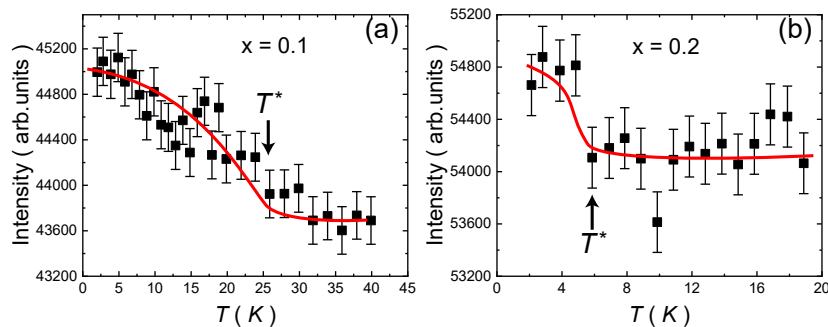


Figure S3. Temperature dependence of the magnetic peak intensity at  $q = (0.5, 0.5, 0)$  in the sample with  $x = 0.1$  in (a) and  $x = 0.2$  in (b). The curves are guides to the eye and the cross-over temperature is defined as the point where the signal above background becomes significant, which implies errors of up to 3 K in these cases.

### C. The cross-over temperature $T^*$ from neutron diffraction

For the samples showing no phase transition into an ordered phase, in Fig. 4 we have indicated a temperature  $T^*$  where both the  $\mu$ SR and neutron data show the onset of significant short-range correlations. It should be noted that, strictly speaking,  $T^*$  can not be defined unambiguously or uniquely as it merely signifies a sharp cross-over. Therefore,  $T^*$  determined from the neutron-diffraction measurements is not necessarily exactly equal to that from the  $\mu$ SR data, since these two techniques measure the system in different ways and with very different energy resolution. We here show that both experiments nevertheless produce compatible results for  $T^*$ .

Figures S3(a) and S3(b) show the temperature dependence of the magnetic peak intensity measured with neutron diffraction at wave-vector  $q = (0.5, 0.5, 0)$  (corresponding to Néel AFM order) for the  $x = 0.1$  and  $x = 0.2$  samples, respectively.  $T^*$  is determined to be the temperature where a signal is detected above the high- $T$  background, which is  $T^* \approx 25$  and  $T^* \approx 6$  K, respectively, for  $x = 0.1$  and  $x = 0.2$ , with rather large error bars of 2-3 K due to the weak signal. Comparing with the  $\mu$ SR result for  $x = 0.1$  in Fig. 4, the results agree well. We do not have  $\mu$ SR results for  $x = 0.2$ .

## 2. CRITICAL SCALING OF THE RELAXATION RATE

As discussed in the main paper, the  $x = 0.05$  and  $0.1$  samples exhibit quantum-critical scaling in the  $\mu$ SR relaxation rate and are candidates for the RS state at low temperatures. According to QMC simulations of a “designer model” realizing the RS phase in a 2D quantum magnet [22, 23], this state is critical with large dynamic exponent,  $z \geq 2$ , with  $z = 2$  at the transition from the Néel state and  $z$  increasing upon moving into the RS phase, and with dominant Néel type spin correlations decaying with distance  $r$  as  $r^{-2}$  universally. This correlation function formally implies that the exponent  $\eta$  in the standard form [36] of the quantum-critical correlation function for a system in  $d$  space dimensions,

$$C(r) \propto r^{-(d+z-2+\eta)}, \quad (\text{S2})$$

depends on  $z$  through the relationship  $\eta = 2 - z$ . Thus, in the RS state this exponent is negative, which is normally not possible in uniform systems but is not uncommon in disordered systems.

The exponent  $\eta$  appears also in dynamical scaling forms, e.g., the NMR relaxation rate  $1/T_1$  scales as  $T^\eta$  at the O(3) quantum-critical point in uniform antiferromagnets, where  $z = 1$  [37]. One can expect the  $\mu$ SR relaxation rate  $\lambda$ , which like  $1/T_1$  depends on local low-energy spin fluctuations, to scale in the same way. However, since the dynamic exponent  $z \neq 1$  in the RS state, the  $T^\eta$  form has to be modified as follows: The correlation length in a quantum-critical system scales as  $\xi \propto T^{-1/z}$ , and we can therefore formally express the temperature as  $T \propto \xi^{-z}$ . For  $z = 1$ , we can write  $\lambda \propto T^\eta \propto \xi^{-\eta}$ , and the generalization to  $z \neq 1$  is obtained by inserting the correct  $T$ -dependent expression for the correlation length. Thus,  $\lambda \propto \xi^{-\eta} \propto T^{\eta/z}$ . Using the form  $\eta = 2 - z$  in the RS state, we expect  $\lambda \propto T^{-\gamma}$ , where we have defined the positive exponent  $\gamma = 1 - 2/z$ , with  $z \geq 2$ . This is the exponent that was extracted from the data fits in Fig. 3(d).

The asymptotic scaling form of  $\lambda(T)$  can also be derived in a more transparent way: First, consider the well known NMR spin-lattice relaxation rate  $1/T_1$ , which for a spin-isotropic system is given by [57]

$$\frac{1}{T_1} = \frac{\gamma^2}{2} \sum_{\mathbf{q}} A^2(\mathbf{q}) S(\mathbf{q}, \omega_N), \quad (\text{S3})$$

where  $\gamma$  is the gyromagnetic ratio,  $A_{\mathbf{q}}$  is the Fourier transform of the hyperfine constants describing the coupling between the nuclear and electronic spins, and  $\omega_N$  is the field-dependent nuclear resonance frequency. The hyperfine coupling is short-ranged in space, and if the nucleus considered is in the ion hosting the localized electronic spins (e.g., Cu NMR in the material considered here), it is often sufficient to consider purely local on-site interactions  $A_0$ , so that the momentum sum in Eq. (S3) reduces to  $A_0^2 S_0(\omega_N)$ , where  $S_0(\omega)$  is the on-site (single-spin) dynamic structure factor.

Typically, the resonance frequency is much lower than other energy scales in the system, and the zero-frequency limit can be considered (unless there are significant spin diffusion contributions, which can cause low-frequency divergencies).

Thus, with these simplifications, which are often completely valid, the relaxation rate is proportional to  $S_0(\omega \rightarrow 0)$  (with prefactors that are known or can be measured). Since  $\mu\text{SR}$  also is a probe of low-frequency local spin fluctuations, we expect the same form;

$$\lambda \propto S_0(\omega \rightarrow 0). \quad (\text{S4})$$

The local dynamic spin structure factor  $S_0(\omega)$  (and also its  $q$  dependent variant) can be calculated in various analytical approximative schemes or numerically; for example, it was calculated in the case of the 1D RS state in Ref. 58. However, the low-frequency limit is often challenging, especially in QMC calculations, where the corresponding imaginary-time dependent spin correlation function  $G_0(\tau)$  has to be calculated and analytically continued to real frequency. To circumvent the latter step, Randeria et al. suggested a very useful approximation [59], which was expressed in a slightly different form in Ref. 58. Neglecting unimportant factors, the approximation amounts to

$$S_0(\omega \rightarrow 0) \propto \frac{1}{T} G_0(\tau = \beta/2), \quad (\text{S5})$$

and then the relaxation rate Eq. (S4) is approximated as

$$\lambda \propto \frac{1}{T} G_0(\tau = \beta/2), \quad (\text{S6})$$

where  $\beta = 1/T$ . Here we will use this form, which is expected in general to become better with decreasing  $T$ , to derive the critical scaling behavior of  $\lambda$  in the RS phase.

As already mentioned above, a quantum-critical spatial correlation function is conventionally written as Eq. (S2), where  $d = 2$  in our case. The on-site correlation in imaginary time is modified by the dynamic exponent [36]

$$G_0(\tau) \propto \tau^{-(d+z-2+\eta)/z}, \quad (\text{S7})$$

reflecting that space and (imaginary) time distances are related as  $\tau \sim r^z$ , which is used to obtain Eq. (S7) from Eq. (S2). Thus, in the RS state with the staggered spatial spin correlation function  $C(r) \propto r^{-2}$ , the time correlations take the form  $G_0(\tau) \propto \tau^{-2/z}$ . Using this form in Eq. (S6) immediately gives the scaling form  $\lambda \propto T^{-(1-2/z)}$ , in agreement with the result presented earlier. The fact that we observe this kind of scaling with  $z > 2$ , Fig. 3(d), with  $z$  also increasing upon moving further away from the Néel phase as predicted [22], constitutes strong support for an RS phase in  $\text{Sr}_2\text{CuTe}_{1-x}\text{W}_x\text{O}_6$ .

### 3. 2D HEISENBERG MODEL

For the Monte Carlo simulations of the classical Heisenberg models, we used methods that have been previously explained in detail in the literature [46, 47]. The simulations combine heat-bath sweeps with energy conserving ‘‘over-relaxation’’ updates. We found the latter to be particularly important for reaching the ground state of systems with a small number of

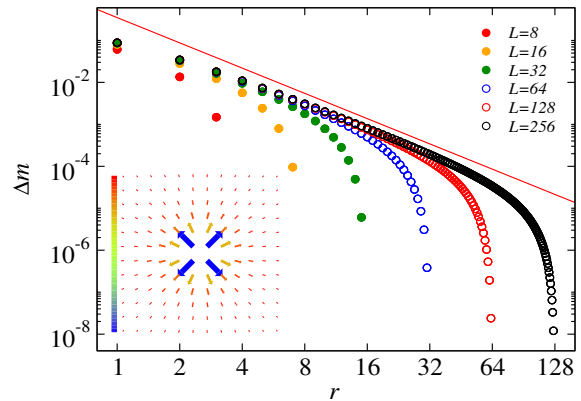


Figure S4. Plaquette impurity induced deformation of the Néel order parameter for different system sizes, as in Fig. 5 but with  $J'_2 = 0$ .

W-type impurities. In all simulations, we started at a high temperature and gradually lowered the temperature in order to alleviate problems with long autocorrelation times. For the systems with more than one W impurity (random mixes of Te and W plaquettes) disorder averages were taken over hundreds of realizations of random locations of the impurities.

In Fig. 5 in the main text we demonstrated an impurity induced deformation of the sublattice magnetization that decays with the distance  $r$  from the impurity as  $1/r^2$ . This decay implies that the total response of a single impurity diverges logarithmically with increasing system size. We here provide additional results demonstrating that the order parameter indeed vanishes for any concentration  $x > 0$  of the impurities.

In the main paper, the Monte Carlo simulations were carried out with parameters approximating those estimated [33] for  $\text{Sr}_2\text{CuTe}_{1-x}\text{W}_x\text{O}_6$ . The bulk parameters for  $x = 0$ , illustrated in Fig. 1(a), were  $J_1 = 1$  and  $J'_2 = 0.1$ . Even with the small frustrating  $J'_2$  terms, the  $T = 0$  order parameter is the fully collinear Néel state, and we do not expect that the frustration is in any way required to obtain the  $r^{-2}$  decay of the deformation. To explicitly demonstrate that the classical Heisenberg model with only the first-neighbor couplings  $J_1$  also has the same impurity response as in Fig. 5, here in Fig. S4 we show simulation results for  $J'_2 = 0$ . These results confirm that the  $r^{-2}$  form emerges as the system size increases.

The  $1/r^2$  form with no angular dependence of the deformation of the order parameter may appear surprising in light of there being no such monopole-like solution of the Poisson equation, which provides the long-distance continuum description of the Néel state with impurities [60]. As will be discussed in more detail elsewhere [61], the plaquette impurity considered here can be regarded as a composite of two dipoles, with the relative angle of the deformation vectors in the  $xy$  plane chosen to minimize the energy. The angular degree of freedom of the deformation is missing in treatments of impurities in long-range ordered systems of spins with only two components [62].

For the following results we go back to  $J'_2 = 0.1$ , and we expect the same kinds of behaviors also for  $J'_2 = 0$ . In Fig. S5(a) we show results for the disorder-averaged  $T = 0$

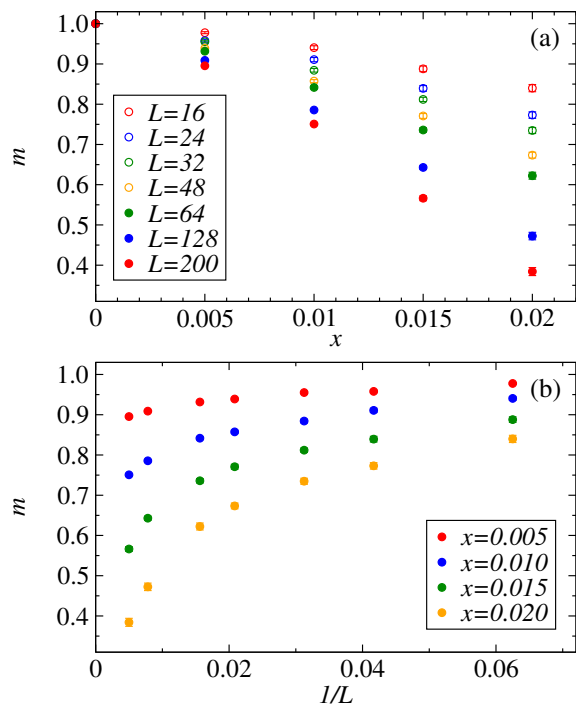


Figure S5. (a) Disorder averaged order parameter versus the concentration of W-type plaquette impurities, graphed for several system sizes. (b) Order parameter at several fixed impurity concentrations  $x$  graphed vs the inverse system size.

Néel order parameter  $m$  versus the concentration of impurities. Increasing the system size consistently leads to a smaller value of  $m$ . In Fig. S5(b) we show results versus the inverse system size for several low impurity concentrations. Here we can observe that  $m$  always decreases with increasing  $L$ . Given the logarithmic singularity suggested by the single-impurity response, the most natural scenario is that  $m$  vanishes in the thermodynamic limit for all  $x > 0$ , but it is difficult to demonstrate that reliably using results such as those in Fig. S5, because of the logarithmic-type singularity that makes extrapolations difficult.

A better way to investigate the presence or absence of order for small  $x$ , introduced in Ref. 5, is to consider a system with a single impurity to have concentration  $x = 1/L^2$ , and to compute the initial slope,

$$R = \frac{dm}{dx}, \quad (\text{S8})$$

of the order parameter vs  $x$  based on this value;

$$R_1(L) = L^2[1 - m_1(L)], \quad (\text{S9})$$

where  $m_1$  is the value of  $m$  computed with the single impurity (averaged over the entire system). Then, if indeed  $m = 0$  for  $L \rightarrow \infty$  at  $x = 0^+$ , the slope  $R_1(L)$  will diverge. In order to take into account possible subtle interaction effects, we here additionally use a modified approach with  $L$  randomly placed impurities in the  $L^2$  system, for which the concentration is  $x = 1/L$  and the slope is

$$R_L(L) = L[1 - m_L(L)], \quad (\text{S10})$$

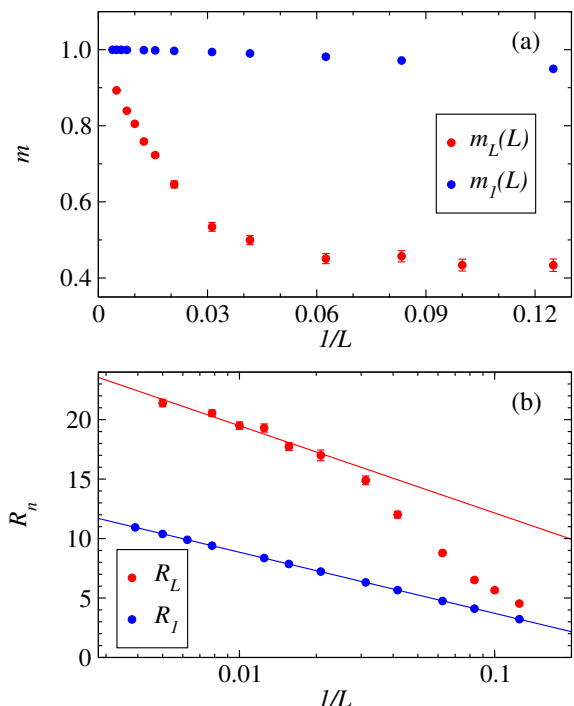


Figure S6. (a) Néel order parameter vs inverse system size in systems with a single impurity (blue symbols) and with  $L$  impurities (red symbols), graphed versus the inverse of the system size  $L$ . (b) Slope graphed on a log-linear plot of the magnetization curve at  $x = 0$  based on the size-dependent definitions, Eqs. (S9) and (S10), with the data in (a). The lines are fits corresponding to the logarithmically divergent forms  $R_n(L) \sim a_n + b_n \log(L)$  with both definitions (with systems containing  $n = 1$  and  $n = L$  impurities).

where  $m_L(L)$  is the impurity-averaged order parameter for  $L$  impurities in the lattice with  $L^2$  spins.

In Fig. S6(a) we show  $m_1(L)$  and  $m_L(L)$  versus  $1/L$ . In the former, we can see clearly the expected approach to the fully saturated bulk order parameter  $m = 1$  when  $L$  increases. For  $m_L(L)$  we also have to asymptotically approach the same limit, and this appears plausible though the convergence is slower, as expected, because of the higher concentration  $x$  for a given system size. In Fig. S6(a) we graph the initial slopes defined in Eqs. (S9) and (S10). Both quantities diverge logarithmically, confirming that the impurity response in the  $x \rightarrow 0$  limit has a logarithmic singularity. Any other interpretation than  $m(x) = 0$  for all  $x > 0$  is then unlikely, as indicated also by the results in Fig. S6 for small but finite impurity concentrations.

The Néel order suppression for any  $x > 0$  is also supported by the strong sensitivity of  $T_c(x)$  to the 3D coupling  $J_\perp$  in Fig. 4(b), which suggests that the transition into the ordered phase at  $x > 0$  and  $T > 0$  is due to the inter-layer effect. It would be interesting to also study the deformation induced by a single-impurity in the 3D coupled-layer system, but we have not yet done so. We should expect the  $1/r^2$  decay to be cut off at some distance depending on  $J_\perp$  (diverging as  $J_\perp/J_1 \rightarrow 0$ ) and, therefore, the slopes defined in Eqs. (S9) and (S10) to be finite for any  $J_\perp > 0$ .

Related issues were recently discussed by Dey et al. in the context of a host system (the Heisenberg model on the triangular lattice) with coplanar AFM order [8]. While previous works have considered destruction of long-range order by dipolar impurities in two-component spin systems (the XY model) [62], this system lacks the rotational degree of freedom of the distortion field of impurities in the Heisenberg

case. The lack of previous works on the plaquette impurity (which, as we pointed out, can be regarded as a composite of two dipoles at a certain relative angle) likely reflects the absence of experimental motivation before the investigations of  $\text{Sr}_2\text{CuTe}_{1-x}\text{W}_x\text{O}_6$  demonstrated these particular coupling patterns [30–33].